Structure–function relationship in annexin A13, the founder member of the vertebrate family of annexins

Javier TURNAY*, Emilio LECONA*, Sara FERNÁNDEZ-LIZARBE*, Ana GUZMÁN-ARÁNGUEZ*, María Pilar FERNÁNDEZ†, Nieves OLMO* and M[a] Antonia LIZARBE*[1]

*Departamento de Bioquímica y Biología Molecular I, Facultad de Ciencias Químicas, Universidad Complutense, 28040-Madrid, Spain, and †Departamento de Bioquímica y Biología Molecular, Facultad de Medicina, Universidad de Oviedo, 33006-Oviedo, Spain

Annexin A13 is considered the original progenitor of the 11 other members of vertebrate annexins, a superfamily of calcium/phospholipid-binding proteins. It is highly tissue-specific, being expressed only in intestinal and kidney epithelial cells. Alternative splicing generates two isoforms, both of which bind to rafts. In view of the lack of structural information supporting the physiological role of this annexin subfamily, we have cloned, expressed and purified human annexin A13b to investigate its structural and functional properties. The N-terminus of annexin A13b: (i) destabilizes the conserved protein core, as deduced from the low melting temperature in the absence (44 °C) or presence of calcium (55 °C), and (ii) impairs calcium-dependent binding to acidic phospholipids, requiring calcium concentrations $> 400\ \mu$M. Truncation of the N-terminus restores thermal stability and decreases the calcium requirement for phospholipid binding, confirming its essential role in the structure–function relationship of this annexin. Non-myristoylated annexin A13b only binds to acidic phospholipids at high calcium concentrations. We show for the first time that myristoylation of annexin A13b enables the direct binding to phosphatidylcholine, raft-like liposomes and acidic phospholipids in a calcium-independent manner. The conformational switch induced by calcium binding, from a 'closed' to an 'open' conformation with exposure of Trp^{227}, can be mimicked by a decrease in pH, a process that may be relevant for membrane interactions. Our studies confirm that the common structural and functional characteristics that are dependent on the protein core of vertebrate annexins are likely to be common conserved features, whereas their variable N-termini confer distinct functional properties on annexins, as we report for myristoylation of annexin A13b.

Key words: annexin A13, calcium binding, CD spectroscopy, fluorescence spectroscopy, phospholipid binding, thermal stability.

INTRODUCTION

The annexin superfamily comprises a group of calcium- and phospholipid-binding proteins characterized by a common structural arrangement, the annexin core. This core is defined by a tetrad structure of homologous internal repeats that mediates the reversible calcium-dependent binding to biological membranes [1–3]. It is composed of four repeats [eight in AnxA6 (annexin A6)] universally conserved throughout annexin evolution [4,5]. Each of them is formed by a four anti-parallel α-helix (A, B, D and E) bundle capped by helix C, as assessed from the crystal structure of several family members. The four domains arrange around a central hydrophilic pore giving rise to a slightly bent disc with calcium- and membrane-binding sites located to the convex side [6]. Calcium binds mainly to the well characterized type II calcium-binding sites [1–3]. However, additional calcium- and phospholipid-binding sites have been described, highlighting the complexity of annexin interactions with membranes [7,8]. In contrast with the conserved core, the N-terminus is variable in both length and amino acid sequence, and is considered to be a major regulatory region of annexins [9,10].

AnxA13 is a key member of vertebrate annexins. The relationship of its gene organization with that of protists and plants indicates that it is the most ancient member of vertebrate annexins [11]. The consequent evolutionary steps originate the other members of the family, beginning with the duplication to AnxA7 and AnxA11 [12–14]. A short 'a' isoform was first identified as a gut-specific annexin by Wice and Gordon [15]; alternative splicing at the N-terminus originates the 'b' isoform, with an insertion of 41 residues [16]. Another peculiar feature of this subfamily is the presence of an N-terminal sequence that leads to the N-myristoylation of the terminal glycine residue, a post-translational modification that is unique among vertebrate annexins.

Functionality of annexins has been widely discussed. Several *in vitro* roles have been assigned to these proteins, such as anti-coagulatory and anti-inflammatory activities, involvement in calcium signal transduction, membrane fusion, and endo- and exocytosis, as well as calcium channel regulation, although their *in vivo* functions are just beginning to be understood [1–3]. This functional diversity can be attributed to specific gene regulation, expression patterns or subcellular localization. It can be also explained in terms of differences in the N-terminal region which mediates the interaction with other proteins, undergoes several post-translational modifications and influences the overall structure of the protein [9,10]. Most of these observations are based on the calcium-dependent binding to membranes; however, a lot of attention is being focused lately on the possible calcium-independent interaction of annexins with phospholipids and on the influence of mildly acidic pH on the structure and possible insertion of annexins into the bilayer.

The specific role of AnxA13 is of particular interest, as its expression is limited to epithelial cells and its localization is also specific. The AnxA13a isoform localizes to both apical and

Abbreviations used: Anx, annexin; CCA, convex constraint algorithm; IPTG, isopropyl β-D-thiogalactoside; LB, Luria–Bertani; MALDI–TOF MS, matrix-assisted laser-desorption ionization–time-of-flight mass spectrometry; PC, phosphatidylcholine; PG, phosphatidylglycerol; PS, phosphatidylserine; T_m, melting temperature; λ_{ex}, excitation wavelength.

[1] To whom correspondence should be addressed (email lizarbe@bbm1.ucm.es).

basolateral membranes, but AnxA13b is enriched in the apical region in the lower three-quarters of the microvilli of polarized epithelial cells [17,18]. Moreover, both isoforms associate with detergent-resistant lipid microdomains, the so-called rafts. In good agreement with these results, AnxA13a has been implicated in both apical and basolateral transport, while AnxA13b only takes part in apical transport [19,20]. N-myristoylation appears to be essential for these roles, whereas calcium seems to be required only for the association of AnxA13a to basolateral transport vesicles. The co-localization of AnxA13b with KIFC3, a minus-end-directed motor, supports further the participation of this protein in the formation and docking of vesicles from the *trans*-Golgi network to the apical membrane [19,21]. Furthermore, AnxA13b interacts with Nedd4, directing it to the apical membrane and to raft microdomains [22].

In the present study, we performed a structural characterization of AnxA13b considering the effect of calcium binding, the main modulator of its activity. Taking into account that mildly acidic pH values trigger important conformational changes in Anx A5 and *Hydra* AnxB12, we have also analysed the effect of increasing proton concentration on AnxA13b structure. Additionally, we have been able to obtain the protein core of AnxA13 as well as the myristoylated AnxA13b in order to characterize the binding properties of these proteins with different phospholipid vesicles. As we have mentioned before, AnxA13 is the key between the 'A' family and the rest of annexins; it is therefore worth studying the structural and functional characteristics of this annexin in order to determine whether some of the common properties of these proteins result from a convergent evolution or rather they constitute a shared and conserved property maintained throughout evolution.

EXPERIMENTAL

Construction of AnxA13b expression vector

The sequence for human AnxA13b cDNA has been completed and annotated previously (IMAGE: 3349423; GenBank® accession number AJ306450). This sequence, encoding the full-length cDNA, was used as template to amplify and isolate the coding portion by PCR. Oligonucleotide primers 22 bp long were synthesized according to the published sequence for both ends of the coding cDNA. The oligonucleotide sequences included created NcoI and HindIII restriction sites to facilitate the insertion of coding cDNA into the expression plasmid pTrc99A (Amersham Biosciences, Bucks., U.K.). The identity of the final construct pTrcA13Hb was verified by DNA restriction analysis and sequencing.

Protein expression and purification

JA221 *Escherichia coli* cells were transformed with the human AnxA13b expression construct pTrcA13Hb and grown in LB (Luria–Bertani) broth containing 100 μg/ml ampicillin at 37 °C until a D_{600} of 0.5 was reached. Optimal expression induction was obtained by addition of 1 mM IPTG (isopropyl β-D-thiogalactoside) for 3 h at 37 °C. Purification of the recombinant protein was achieved by taking advantage of the property of being able to reversibly interact with PS (phosphatidylserine) vesicles and following, with slight modifications, the method described for AnxA5 [23]. Briefly, after centrifugation at 6000 ***g*** for 15 min, collected cells were resuspended in 50 mM Tris/HCl, pH 7.4, containing 0.1 M NaCl, 2.5 mM EGTA and 2 mM PMSF and ruptured by sonication cycles at 4 °C. The homogenate was stirred at 4 °C for 90 min and centrifuged at 27 000 ***g*** for 90 min at 4 °C. The supernatant was mixed with PS-enriched vesicles (bovine brain extract with approx. 80 % PS; 1 mg/ml final concentration; Sigma, Alcobendas, Spain) and 2 mM $CaCl_2$, and stirred for 30 min at 4 °C. The mixture was centrifuged at 27 000 ***g*** for 45 min at 4 °C, and the pellet washed twice with 50 mM Tris/HCl, pH 7.4, containing 0.1 M NaCl and 2 mM $CaCl_2$. The recombinant protein was then extracted by resuspension of the vesicles in the presence of 50 mM Tris/HCl, pH 7.4, containing 5 mM EGTA and 0.25 M NaCl, and further centrifugation at 27 000 ***g*** for 45 min at 4 °C. Finally, the protein was purified, after dialysis against 50 mM Tris/HCl, pH 7.4, and 1 mM EGTA, by DEAE-cellulose chromatography; AnxA13b was eluted using buffer containing 0.25 M NaCl and 1 mM EGTA.

Limited proteolysis of AnxA13b was performed in 50 mM Tris/HCl, pH 8.0, and 0.1 M NaCl with sequence-grade tosylphenylalanylchloromethane-treated trypsin (Roche Diagnostics, Mannheim, Germany) at an enzyme/substrate ratio of 1:1000 (w/w) at 25 °C for 2 h. The reaction was stopped by the addition of 1 mM PMSF, and the truncated protein ($AnxA13^{core}$) was purified by size-exclusion chromatography on a Sephadex G-75 column (Amersham Biosciences).

The identity of the recombinant (AnxA13b) and N-terminally truncated ($AnxA13^{core}$) proteins was confirmed by amino acid analysis (Beckman 6300 amino acid analyser) as described previously [23], as well as N-terminal sequencing and MALDI–TOF MS (matrix-assisted laser-desorption ionization–time-of-flight mass spectrometry). The molar absorption coefficient at 280 nm was determined from the UV/visible spectrum after subtraction of apparent absorption due to light scattering and determination of the protein concentration by amino acid analyses from aliquots directly taken from the cuvette ($\varepsilon^{0.1\%} = 0.81$ and 0.75 ml $\cdot$ mg^{-1} $\cdot$ cm^{-1} for AnxA13b and $AnxA13^{core}$ respectively).

Myristoylation of recombinant AnxA13b was performed in JA221 *E. coli* cells harbouring plasmid constructs encoding N-myristoyltransferase from *Saccharomyces cerevisiae* (pBB131 containing the gene for kanamycin resistance and also inducible by IPTG [24]; kindly provided by Dr J. I. Gordon, Department of Molecular Biology and Pharmacology, Washington University School of Medicine, St. Louis, MO, U.S.A.) and human AnxA13b. Cultures of the double transformants were shaken at 37 °C to a D_{600} of 0.5 in LB broth containing 100 μg/ml ampicillin and 100 μg/ml kanamycin sulphate. Simultaneous expression of both recombinant proteins was triggered by the addition of 1 mM IPTG for 4 h at 37 °C. Protein radiolabelling was assessed by simultaneous addition of IPTG and [9,10(n)-^{3}H]myristic acid (Amersham Biosciences) (55.0 Ci/mmol, 10 μCi/ml of culture). Non-myristoylated AnxA13b was mainly solubilized as described above, whereas the myristoylated protein ($AnxA13b^{myr}$) remained in the pellet from the bacterial homogenization. Solubilization was achieved by addition of 2 % (w/v) octylglucoside; partial purification was performed by DEAE-cellulose chromatography after dialysis against 50 mM Tris/HCl, pH 7.4, containing 0.5 % (w/v) octylglucoside, and elution with increasing NaCl concentration. Finally, octylglucoside was removed by exhaustive dialysis against 50 mM Tris/HCl, pH 7.4, and 0.1 M NaCl, as described previously [25].

CD spectroscopy

The far-UV CD spectra were monitored between 195 and 260 nm at 20 °C in a Jasco J-715 spectropolarimeter equipped with a Neslab RTE-111 thermostat using 0.01 or 0.05 cm path-length thermostatically controlled cuvettes. All spectra were averaged over at least six scans and were corrected by subtracting buffer contribution from parallel spectra in the absence of protein; units are expressed as mean residue weighed molar ellipticities

($[\theta]_{MRW}$). Prediction of the secondary structure from the far-UV CD spectra was performed using the CCA (convex constraint algorithm) as described by Perczel et al. [26]. Melting curves were obtained after dialysis of the samples against 20 mM Hepes, pH 7.4, containing 0.1 M NaCl to avoid pH changes during heating. Changes in ellipticity at 208 nm were monitored between 20 and 85 °C at 60 °C/h. Ellipticity data were converted into the apparent fraction of unfolded protein (F_{app}) and plotted against temperature according to $F_{app} = (\theta_{obs} - \theta_N)/(\theta_U - \theta_N)$, where θ_{obs} is the observed ellipticity value at a given temperature, and θ_N and θ_U are the values for native and unfolded forms respectively, determined at each temperature by linear extrapolation of the native and unfolded baselines.

The effect of calcium on the far-UV CD spectrum and melting temperature (T_m; considered as the midpoint of the unfolding transition calculated from the plot of F_{app} against temperature) was analysed employing protein samples with increasing $CaCl_2$ concentrations. Samples with equivalent maximal ionic strength, obtained by the addition of NaCl or $MgCl_2$ instead of $CaCl_2$, were used as controls. Control samples without calcium always contained 1 mM EGTA. The effect of acidic pH was studied by dilution of a concentrated protein stock with 20 mM sodium citrate buffer containing 0.1 M NaCl at different pH values [27], and the exact pH values after dilution were determined using a microelectrode. Spectra in the presence of pure brain-extract PS liposomes (50 nm in diameter, obtained by extrusion as described below; 800:1 PS/protein molar ratio) were recorded in the absence or presence of 750 μM $CaCl_2$ or $MgCl_2$ using a 0.01 cm path-length cuvette to minimize artifacts arising from light scattering.

Fluorescence emission spectroscopy

Fluorescence emission spectra were recorded in an SLM Aminco 8000C spectrofluorimeter at 20 °C. Global and tryptophan emissions were measured separately with excitation wavelengths of 275 and 295 nm respectively, using a 0.4 cm excitation path-length and 1.0 cm emission path-length cuvette. Spectra were monitored between 265 and 420 nm for global emission or 305 and 420 nm for tryptophan emission. Rayleigh scattering at 90° was obtained from the maximum at 275 nm of spectra recorded at this excitation wavelength. The emission spectrum from tyrosine residues was determined after subtracting the contribution of the tryptophan residue to the global emission spectra [λ_{ex} (excitation wavelength) = 275 nm]; this contribution was obtained by correction of the tryptophan spectrum ($\lambda_{ex} = 295$ nm) using a factor determined from the ratio between both spectra ($F_{ex=275}/F_{ex=295}$) in the range 370–400 nm.

The effect of calcium was titrated by sequential addition of $CaCl_2$ in the absence or presence of 50 nm unilamellar PS vesicles (800:1 PS/AnxA13b molar ratio). The effect of acidic pH was studied as described for CD spectroscopy. Light scattering was minimized by crossed Glan–Thompson polarizers only in spectra obtained in the presence of liposomes.

Acrylamide quenching of tryptophan fluorescence was analysed by recording emission spectra ($\lambda_{ex} = 295$ nm) at increasing acrylamide concentrations, and taking into account the effect of dilution as described previously [23,28]. Care was taken to avoid the inner-filter effect and that solutions always presented UV absorption below 0.04 at 295 nm. The quenching constant (K_{SV}) was calculated from the Stern–Volmer plot of F_0/F at the emission maximum against acrylamide concentration, according to the equation $F_0/F = 1 + K_{SV}[Q]$, where F_0 is the fluorescence intensity at zero quencher concentration, and F is the intensity at a given quencher concentration ([Q]).

Binding to phospholipids and vesicle aggregation assays

Unilamellar vesicles were prepared using natural lipids (purity > 99 %): PS (bovine brain) (Avanti Polar Lipids, Alabaster, AL, U.S.A.), PC (phosphatidylcholine) (egg yolk), PG (phosphatidylglycerol) (derived from egg-yolk PC), and a raft-like mixture (PC/sphingomyelin/cholesterol, 1:1:1) (Sigma). Liposomes were obtained by hydration of a thin dried-lipid film in buffer (50 mM Tris/HCl or 20 mM Hepes, pH 7.4) containing 0.1 M NaCl, followed by extrusion through polycarbonate filters of either 100 or 400 nm pore diameter (Lipex Biomembranes, Vancouver, Canada). Small unilamellar vesicles (50 nm) were prepared from freshly obtained 400 nm vesicles by further extrusion through polycarbonate filters of the corresponding pore diameter.

The interaction of AnxA13b or AnxA13^{core} with 400 nm vesicles was carried out at a constant lipid/protein molar ratio of 800:1 with variable calcium concentrations in 50 mM Tris/HCl, pH 7.4, containing 0.1 M NaCl at 20 °C for 15 min. The final mixture (300 μl) was ultracentrifuged at 110 000 rev./min at 4 °C for 1 h (Airfuge Beckman; A110 rotor). After separation of supernatant and pellet, proteins were detected by Coomassie Blue staining after SDS/PAGE. Phospholipid-free controls showed negligible sedimentation of annexin under these experimental conditions. Gels were scanned, and a densitometric analysis was performed, obtaining volumograms on a photodocumentation system from UVItec (Cambridge, U.K.) and using the UVIBand V.97 software. [^{3}H]Myristoylated AnxA13b binding was analysed as described for the non-myristoylated form; quantification was carried out additionally by measuring radioactivity in supernatants and pellets.

Vesicle-aggregation studies were performed by recording absorption at 360 nm immediately after the addition of calcium to a mixture of unilamellar vesicles (100 nm; 0.1 mg/ml) and AnxA13b at 25 °C. Calcium was added from a $CaCl_2$ stock solution, and absorption was registered in a thermostatically controlled cuvette for at least 10 min.

Structural model

We have generated a three-dimensional model using the Swiss-Model Server version 3.5 (http://swissmodel.expasy.org/) and public X-ray crystallographic data for full-length pig AnxA1, human AnxA2 and AnxA3, human and rat AnxA5, and *Hydra* AnxB12 (Protein Data Bank entries 1MCX, 1XJL, 1AXN, 1ANX, 1A8A and 1AEI respectively), all of them in the 'high-calcium' form to thread the human AnxA13b amino acid sequence into a three-dimensional model for the homologous tetrad core region. Additionally, we have also obtained a structural model for AnxA13b domain III in the absence of calcium using the crystallographic data from pig AnxA1, human AnxA2, bovine AnxA4, and human AnxA5 and AnxA8 (Protein Data Bank entries 1HM6, 1W7B, 1ANN, 1AVH and 1W3W respectively).

Other procedures

SDS/PAGE was performed according to Laemmli [29] using 10 % polyacrylamide gels. Western blotting was performed as described previously [28] using rabbit polyclonal anti-(human AnxA13b) antibodies and a secondary anti-rabbit IgG conjugated with horseradish peroxidase (Bio-Rad, Madrid, Spain). Polyclonal antibodies against recombinant human AnxA13b were raised in rabbits following standard methods. Radioactivity was measured in a Beckman LS 3801 scintillation counter. Autoradiography was performed after soaking the SDS/PAGE gels in the fluorographic reagent Amplify (Amersham Biosciences), drying the gels and exposure to Hyperfilm-MP films (Amersham Biosciences).

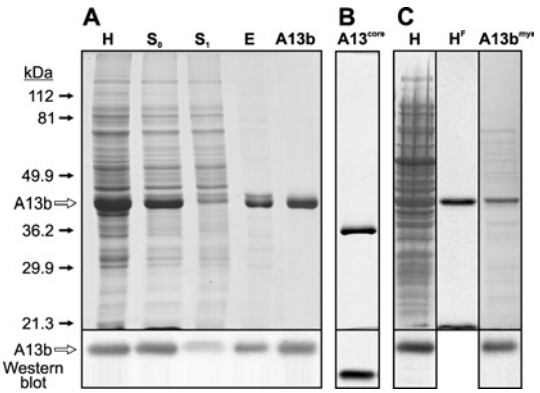

Figure 1 SDS/PAGE analysis of recombinant non-myristoylated and myristoylated AnxA13b expression and purification

(**A**) Expression of AnxA13b was analysed by SDS/PAGE, followed by Coomassie Blue staining and Western blotting. Lane H, bacterial homogenate after protein expression induction; lane S_0, supernatant after centrifugation of the homogenized material in the presence of 2.5 mM EGTA; lane S_1, supernatant after addition of PS-enriched liposomes in the presence of 2 mM $CaCl_2$; lane E, supernatant obtained after extraction with 5 mM EGTA of the complex between AnxA13b and PS-enriched liposomes; lane A13b, pool of fractions obtained after DEAE-cellulose chromatography. (**B**) Lane $A13^{core}$, protein core of AnxA13b. (**C**) Expression of myristoylated AnxA13b was analysed by SDS/PAGE followed by Coomassie Blue staining, fluorography and Western blotting. Lane H, bacterial homogenate after protein induction; lane H^F, fluorography of sample from lane H; lane $A13b^{myr}$, pool of fractions containing purified myristoylated AnxA13b after DEAE-cellulose chromatography and removal of octylglucoside. Molecular masses in kDa and the position of A13b are indicated.

Protein concentration in pure preparations was determined from the UV/visible spectra, except for CD spectroscopy, where quantitative amino acid analysis was used. Regression fitting of the experimental data to different equations was performed using SigmaPlot software version 9.01 obtained from Systat Software (Erkrath, Germany).

RESULTS

Purification of recombinant AnxA13b

The expression of recombinant AnxA13b was studied in JA221 *E. coli* cells transformed with the expression construct pTrcA13Hb. Protein production was high at short induction times (1 mM IPTG), and recombinant AnxA13b was detectable by SDS/PAGE and Coomassie Blue staining (Figure 1A, lane H). Longer times did not yield greater amounts of protein, but were accompanied by a significant increase in protein degradation, as detected by electrophoretic analysis and Western blotting (results not shown). Consequently, 3 h of induction at 37 °C was chosen as the optimal conditions for protein expression.

The electrophoretic and Western blot analyses of the main steps of the purification process are shown in Figure 1(A). Homogenization of the bacterial pellet in the presence of 2.5 mM EGTA (Figure 1A, lane H) allowed the solubilization of the recombinant protein with a high yield (Figure 1A, lane S_0). Sequential addition of multilamellar PS-enriched vesicles and $CaCl_2$ (2 mM final concentration) followed by centrifugation sedimented the recombinant protein, whereas the main part of bacterial proteins remained in the supernatant (Figure 1A, lane S_1). AnxA13b was extracted from the vesicle pellet with buffer containing 5 mM EGTA and 0.25 M NaCl (Figure 1A, lane E); the higher NaCl concentration required to extract the protein from the vesicles emphasizes the importance of ionic interactions in membrane binding [8,30]. The remaining contaminant proteins and phospholipidic vesicles were removed with the DEAE-cellulose chromatographic step (Figure 1A, lane A13b). Controlled trypsin digestion of purified recombinant AnxA13b followed by size-exclusion chromatography yielded $AnxA13^{core}$, a truncated form without the first 48 amino acid residues (cut after Lys^{48}; Figure 1B, lane $A13^{core}$). The identity and purity of the protein preparations were confirmed by Western blotting, N-terminal sequencing (12 residues) and MALDI–TOF MS.

Taking into account that AnxA13b is myristoylated *in vivo*, we considered the production of myristoylated recombinant protein in order to compare its ability to bind to phospholipids with that of the non-myristoylated protein. Figure 1(C) (lane H) shows that the co-transformation of the *E. coli* JA221 strain with pTrcA13Hb and pBB131 yielded recombinant protein that incorporated [^{3}H]myristic acid. Moreover, the only myristoylated protein detected by fluorography was the recombinant annexin (Figure 1C, lane H^F). The myristoylated protein was quite insoluble under the experimental conditions described for the solubilization of non-myristoylated AnxA13b, allowing, in this way, a good separation of both forms of the recombinant protein. The low solubility of the myristoylated protein is probably due to a calcium-independent binding to bacterial membranes. Solubilization using 2 % (w/v) octylglucoside, followed by DEAE-cellulose chromatography and dialysis, yielded final preparations of soluble radiolabelled $AnxA13b^{myr}$ that were approx. 80 % pure (Figure 1C, lane $A13b^{myr}$), and were used for phospholipid-binding experiments.

CD analysis and thermal stability

CD spectra of AnxA13b in the far-UV region in the absence of calcium, at 20 and 85 °C, are shown in Figure 2(A) (continuous lines). The shape of the spectrum at 20 °C reflects a high α-helical percentage in the secondary structure of the protein, with two minima at 208 and 221 nm. Accordingly, the CCA prediction indicates that the main contributions to the secondary structure are α-helix (70–75 %) and random coil (15–18 %), in good agreement with the secondary structure of the protein core of other annexins whose three-dimensional structures are already known. Annexins with a short N-terminus, such as AnxA5 (15 residues), present CD and IR spectra with a prediction of over 80 % α-helical structure [31], whereas AnxA11, with a 200-residue extension in random coil, presents only 29 % α-helix [28]. Taking these data into account, and considering that predictions based on the sequence of the N-terminus of AnxA13b (51 residues) suggest a random coil structure (secondary-structure prediction tools at http://www.expasy.org/tools/#secondary), it can be suggested that the α-helical contribution to the CD spectra corresponds only to the protein core. In fact, truncation of the N-terminus ($A13^{core}$) alters the far-UV CD spectrum, with less negative ellipticity values, but showing a decrease in random coil structures and a parallel increase in α-helical content according to the CCA prediction.

The addition of $CaCl_2$ up to 100 mM induces very slight changes in the CD spectrum of AnxA13b (Figure 2A, broken lines), smaller than those detected in AnxA5 and AnxA11 [28,31], but pointing also to a small increase in α-helix content (< 5 %) and helix length (higher $[\theta]^{220}/[\theta]^{208}$ ratio).

Since the main contribution to the secondary structure is α-helix, thermal denaturation was followed by measuring the molar ellipticity at 208 nm as a function of temperature. The AnxA13b melting curve displays a co-operative transition with a T_m of approx. 44 °C which is approx. 6 °C lower than the value obtained for $AnxA13^{core}$ (Figure 2B, inset). Addition of calcium induces a concentration-dependent increase in the thermal stability of AnxA13b that follows a hyperbolic pattern with a midpoint at

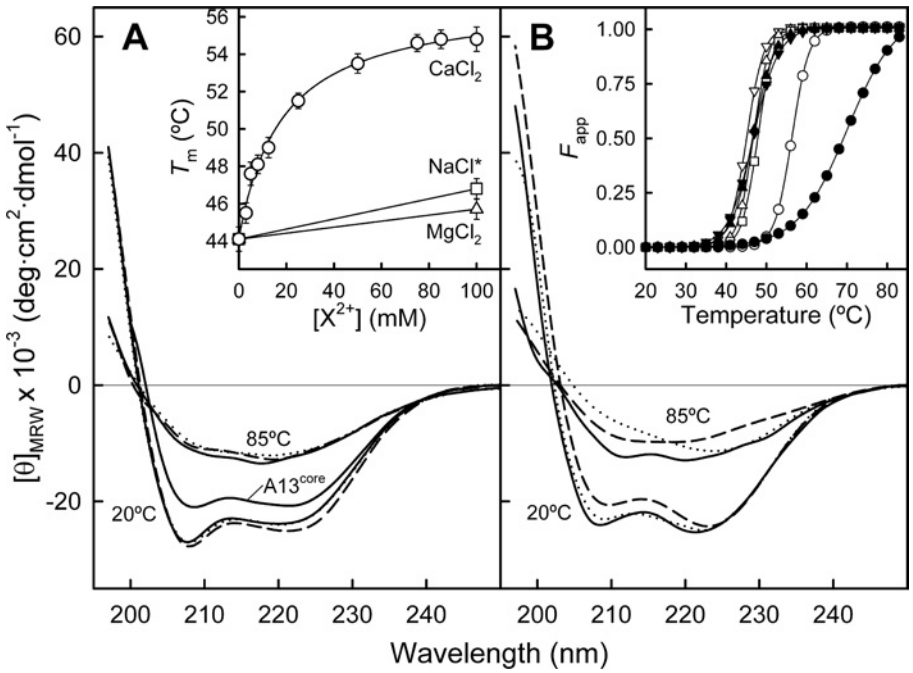

Figure 2 Far-UV CD spectra of AnxA13b in the absence and presence of PS unilamellar vesicles

(**A**) Far-UV CD spectra of AnxA13b (0.3 mg/ml) without calcium (continuous line) and in the presence of 100 mM $CaCl_2$ (broken line) or $MgCl_2$ (dotted line) at 20 and 85 °C are shown. Spectra were registered in 20 mM Hepes, pH 7.4, containing 0.1 M NaCl. Inset: dependence of the T_m on $CaCl_2$ concentration ranging from 0 (1 mM EGTA) to 100 mM (○), 100 mM $MgCl_2$ (△) or NaCl with ionic strength equivalent to buffer containing 100 mM $CaCl_2$ (NaCl*; □). Melting points represent the means ± S.D. for at least two independent determinations. (**B**) Far-UV CD spectra of AnxA13b as described above, but in the presence of 50 nm PS unilamellar liposomes (800:1 lipid/protein molar ratio) without (continuous line) or with 750 μM $CaCl_2$ (broken line) or $MgCl_2$ (dotted line). Inset: apparent fraction of unfolded protein (F_{app}) against temperature (open symbols, in the absence of PS; closed symbols, in the presence of PS vesicles; down triangles, EGTA; circles, $CaCl_2$; up triangles, $MgCl_2$; squares, NaCl).

12.8 mM and a maximum increase of approx. 10–11 °C at concentrations higher than 50 mM (Figure 2A, inset). This effect is calcium-specific and cannot be reproduced by magnesium or by an equivalent increase in ionic strength achieved by addition of NaCl. The study of calcium binding in the absence of phospholipids requires the use of millimolar concentrations of $CaCl_2$, as it is well known that the affinity of annexins for this cation is around three orders of magnitude lower under these conditions [31,32].

Fluorescence emission analysis

Fluorescence emission spectra of AnxA13b were registered with excitation wavelengths of 275 nm (global emission) (Figure 3A) and 295 nm (Trp^{227} emission) (Figure 3B) in the presence of different calcium concentrations. In the absence of calcium, the maximum is around 307 nm and 321 nm for global and tryptophan emission, respectively. Addition of calcium up to 75 mM induces a significant shift in the Trp^{227} maximum towards 344 nm (Figure 3D, inset), whereas only a small shift (from 307 to 303 nm) is detected in the global maximum. When the contribution of tyrosine residues to the global spectra is analysed (Figure 3C, F^{305}, ●), a very slight change in fluorescence intensity at 305 nm is observed, being almost identical to that obtained with $MgCl_2$ (Figure 3C, F^{305}, ○). On the other hand, Trp^{227} emission follows a hyperbolic dependence on calcium concentration in both the position of the maximum and in the ratio between intensities at 344 and 321 nm (Figure 3D). This effect is calcium-specific and is not reproducible by magnesium, with a midpoint effect at 2.7 mM $CaCl_2$ for the F^{344}/F^{321} ratio and 1 mM for the shift in the maximum position. Additionally, we have recorded Rayleigh scattering (Figure 3C, RS^{275}) as a function of calcium or magnesium concentration, and no significant variation has been found, thus indicating that calcium effects are not due to induction of protein aggregation.

The exposure of Trp^{227} to the solvent was studied in the absence and in the presence of 75 mM $CaCl_2$ through analysis of the sensibility of fluorescence emission ($\lambda_{ex} = 295$ nm) to acrylamide quenching up to 170 mM, which does not involve inner-filter effects. Accessibility to acrylamide was confirmed by the decrease in intensity observed in the spectra in both cases, without modification in the position of the maximum (results not shown). The fluorescence emission data at the corresponding maximum (321 or 344 nm) were adjusted according to the Stern–Volmer equation as a function of acrylamide concentration, yielding quenching constants (K_{SV}) of 2.99 and 14.58 M^{-1} in the absence or presence of 75 mM $CaCl_2$ respectively.

Effect of acidic pH on AnxA13b conformation

CD spectra of AnxA13b in the far-UV region were registered at decreasing pH, beginning at 8.0 (Figure 4, continuous line), at approx. 0.1 mg/ml to minimize aggregation of the protein at pH values close to the pI (5.8) or lower. No significant alterations in the secondary structure were detected down to pH 5.0. However, at more acidic pH, changes were observed (Figure 4, upper inset) first in the minimum at 208 nm (down to pH 4.1; Figure 4, broken line) followed by changes at 220 nm (down to pH 2.3; Figure 4, broken/dotted line). The overall changes are reflected in a moderate increase in the $[\theta]^{220}/[\theta]^{208}$ ratio that reaches a maximum at pH 4.1. The decrease thereafter (Figure 4, lower inset) is accompanied by a loss in negative molar ellipticity consistent with an increase in random coil and a parallel decrease in α-helix percentage of approx. 15–20 %.

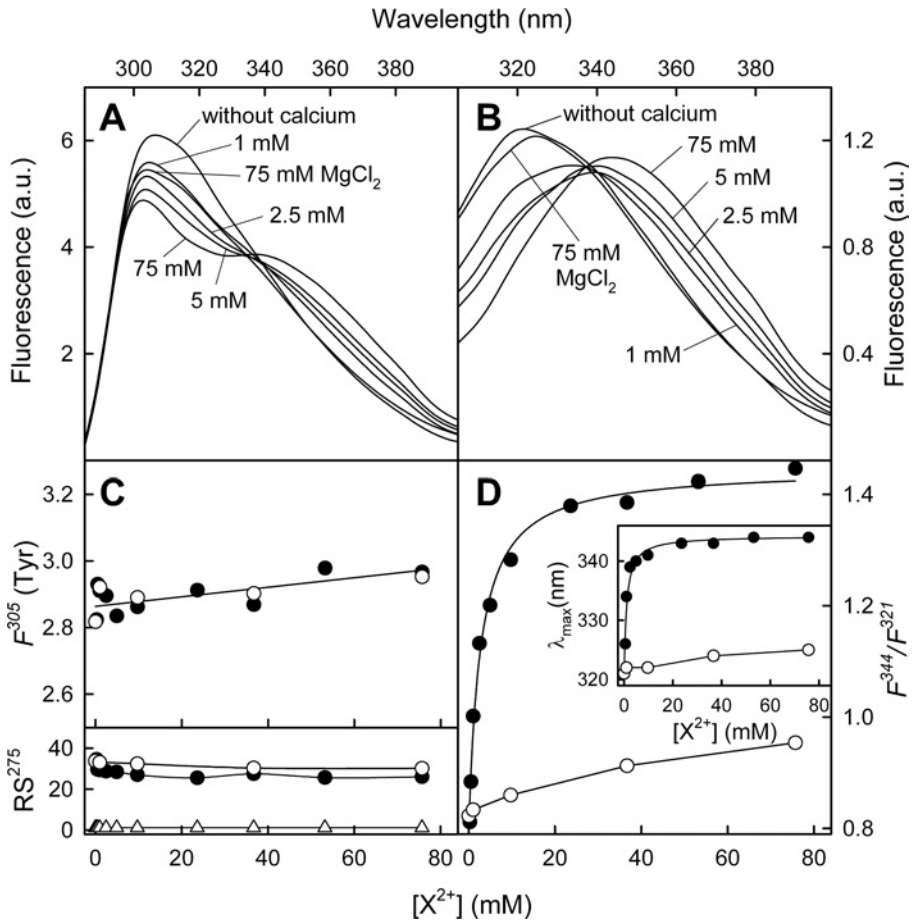

Figure 3 Fluorescence emission spectra of AnxA13b after calcium binding

Emission spectra at excitation wavelengths of 275 (**A**) and 295 (**B**) nm in the absence of calcium or at increasing $CaCl_2$ concentration were registered at 20 °C; protein concentration was 0.2 mg/ml. Only spectra at representative calcium concentrations are shown. Fluorescence is expressed in arbitrary units (a.u.). Variations in the fluorescence intensity of tyrosine residues at 305 nm [F^{305} (Tyr); determined as described in the Experimental section] and in the F^{344}/F^{321} fluorescence intensity ratio of Trp^{227} ($\lambda_{ex} = 295$ nm) with Ca^{2+} (●) or Mg^{2+} (○) concentration are shown in (**C**) and (**D**) respectively. The lower panel in (**C**) represents Rayleigh scattering at 275 nm (RS^{275}) of AnxA13b or buffer (△) at different Ca^{2+} or Mg^{2+} concentrations. The inset in (**D**) shows the variation in the tryptophan fluorescence maximum position with calcium concentration.

Fluorescence emission spectra at excitation wavelengths of 275 and 295 nm were recorded at different pH values (Figures 5A and 5B). The contribution of the 12 tyrosine residues to the global emission spectra was analysed after subtracting that of Trp^{227}. Figure 5(C) (F^{305}) shows the effect of decreasing pH in the fluorescence emission of tyrosine residues at 305 nm. No variations in the intensity were observed from pH 7.8 to approx. pH 4.0, whereas a sharp increase was detected at lower pH values. Fluorescence emission of the unique tryptophan residue ($\lambda_{ex} = 295$ nm) was also affected by pH. Figure 5(D) (inset) shows the shift in the maximum position from 320 nm (pH 7.8) to 340 nm (pH 4.0), with a sigmoid dependence on pH and a midpoint effect at pH 5.9. A similar variation in the F^{340}/F^{321} intensity ratio is observed between pH 6 and pH 4.5 (midpoint at pH 5.8) and a slight decrease below pH 4.

Protein aggregation was studied following Rayleigh scattering at 275 nm (Figure 5C, RS^{275}). No significant increase in scattering was observed from pH 7.8 to 5.0. Thus the changes observed in the Trp^{227} environment at pH 6.5–4.5 are independent of protein aggregation. On the other hand, even though the increase in Rayleigh scattering is simultaneous with the initial increase in tyrosine fluorescence, at pH values below 3, no protein aggregation is detected. Consequently, the increase in tyrosine fluorescence below pH 4 could be the result of a partial protein unfolding (in agreement with CD spectra) and/or a decrease in static quenching due to the loss of negative charge of carboxy groups in the surroundings of tyrosine residues.

Phospholipid binding and vesicle aggregation

The binding of AnxA13b to phospholipid vesicles was studied by ultracentrifugation after incubation of the protein with an excess of large unilamellar vesicles (400 nm in diameter) in the absence (Figure 6B, black bars; 1 mM EGTA) or presence of 500 μM $CaCl_2$ (Figure 6B, white bars). The vesicle pellets and supernatants were analysed by SDS/PAGE (Figure 6A). Figure 6(B) shows that the recombinant protein interacts in a calcium-dependent manner with liposomes composed of acidic phospholipids (PS and PG), but does not bind to PC or raft-like (PC/sphingomyelin/cholesterol, 1:1:1) vesicles. Figure 6(B) also shows the binding of myristoylated (radiolabelled) $AnxA13b^{myr}$ to large unilamellar vesicles. The most interesting finding is that the myristoylated protein binds to PC and raft-like vesicles in a calcium-independent manner, whereas the non-myristoylated form is not able to bind either in the presence or absence of calcium. Additionally, 65–70 % of the binding to acidic

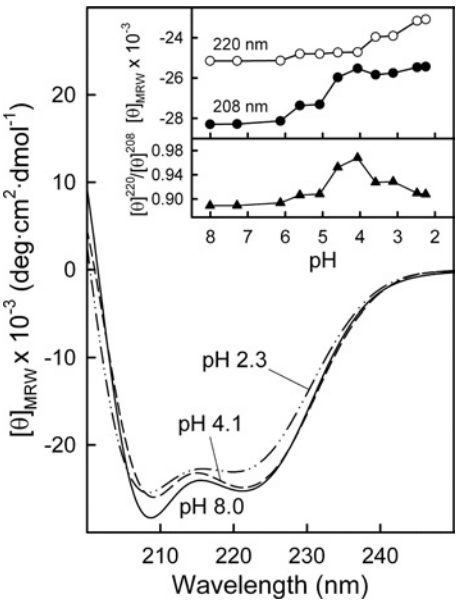

Figure 4 Far-UV CD spectra of AnxA13b as a function of pH

Spectra were recorded at 20 °C using AnxA13b at 0.1 mg/ml in sodium citrate buffer solutions at decreasing pH values, as described in the Experimental section. Only representative spectra at pH 8.0, 4.1 and 2.3 are shown. The inset shows the plot of ellipticity values at 220 and 208 nm against pH (upper panel) and the ratio between these values (lower panel).

phospholipids is also achieved in the absence of calcium, and this process is favoured in the presence of calcium. The ability of $A13b^{myr}$ to bind to membranes in the absence of calcium could explain its insolubility during the purification procedure.

A more detailed analysis of the calcium dependence of AnxA13b, $AnxA13b^{myr}$ and $AnxA13^{core}$ binding to PS vesicles is shown in Figure 6(C). The binding of AnxA13b follows a sigmoid pattern, with a midpoint at 321 μM $CaCl_2$. Calcium requirements for binding of recombinant AnxA13b to PS vesicles are much higher than those described for any other analysed annexin [10]. Surprisingly, removal of the N-terminal extension decreases calcium requirements and $AnxA13^{core}$ shows a midpoint at 53 μM $CaCl_2$, with a total binding at calcium concentrations over 120 μM (Figure 6C). The binding of $AnxA13b^{myr}$ to PS vesicles is also enhanced by addition of calcium.

Binding of AnxA13b to PS has also been analysed by fluorescence emission spectroscopy using unilamellar vesicles (50 nm in diameter) with a constant lipid/protein molar ratio (800:1) and varying $CaCl_2$ concentration (Figure 7). The global emission spectrum ($\lambda_{ex} = 275$ nm) after the addition of PS vesicles in the absence of calcium is quite similar to that registered in the absence of phospholipids, showing a maximum at 307 nm (Figure 7A); however, a slight shift in the Trp^{227} emission ($\lambda_{ex} = 295$ nm) is observed from 321 nm towards 326 nm as well as an approx. 25 % decrease in the quantum yield (Figure 7B, continuous line). The sequential addition of calcium first shifts the Trp^{227} emission maximum towards 340 nm with a midpoint around 324 μM $CaCl_2$ (Figures 7B and 7D, inset), and then induces an increase in the quantum yield that reaches a maximum at approx. 500 μM $CaCl_2$ (Figure 7B). These changes are also reflected in a sigmoid increase in the F^{340}/F^{326} fluorescence ratio that is slightly delayed in comparison with the changes detected in the maximum position (approx. 369 μM $CaCl_2$; Figure 7D, inset). Interestingly, when tyrosine emission spectra are calculated by subtraction of the Trp^{227} contribution to the global spectra, a sigmoid decrease in the intensity at 305 nm is detected with a midpoint at 361 μM $CaCl_2$ (Figure 7C).

Induction of vesicle aggregation was analysed using PS or PG vesicles at different protein and calcium concentrations. No aggregation was induced by the recombinant protein even at high protein (2 μM) or calcium (1 mM $CaCl_2$) concentrations.

Changes in secondary structure after binding of AnxA13b to 50 nm unilamellar PS vesicles were studied by CD spectroscopy. In the presence of EGTA, the spectrum presents a different shape than in the absence of vesicles (Figures 2A and 2B, continuous lines); this change could be the result of either light scattering due to the presence of liposomes or an actual increase in α-helical content or length. In any case, addition of calcium (750 μM) induces a further spectral change (Figure 2B, broken line) and a great increase in the T_m (69 °C; Figure 2B, inset) that is neither induced by magnesium nor accompanied by an increase in light scattering. Taking into account that CCA does not predict significant changes in secondary-structure percentages, the changes in the CD spectrum after PS binding may correspond to an increase in the length of α-helices.

Structural model

We have developed a three-dimensional model of AnxA13b in the calcium-bound form and a model for domain III in the calcium-free conformation in order to analyse whether the stabilizing interactions and conformational changes described for other annexins, mainly AnxA5, have an equivalence in AnxA13b (Figure 8).

It has been described that the equilibrium between the 'closed' calcium-free conformation in domain III of AnxA5 and the 'open' conformation acquired when calcium is bound, depends strongly on a few specific interactions that stabilize the closed conformation: hydrogen bonds between Asp^{226} and Thr^{229}, and between Thr^{224} and Trp^{187}, and a salt bridge between Asp^{190} and Lys^{193} [27, 33,34]. According to the sequence alignment between AnxA5 and AnxA13b, and taking into account the structural model proposed for the latter, AnxA13b can only establish hydrogen bonds between Glu^{266} and Thr^{269} and between the carbonyl oxygen of Ala^{264} and Trp^{227}; AnxA13b presents alanine residues (Ala^{233} and Ala^{264}) in positions equivalent to Lys^{193} and Thr^{224} in AnxA5, and thus some of these stabilizing interactions cannot be established (Figure 8A). The Figure also shows the four tyrosine residues (220 and 243, exposed, and 253 and 273, buried; according to Swiss PDB viewer version 3.7 prediction) present in domain III of AnxA13b and the residues in equivalent positions in AnxA5.

The only tryptophan residue in AnxA13b (Trp^{227}) is located within the IIIA–IIIB loop, in an equivalent position to Trp^{187} in AnxA5, Trp^{186} in AnxA4 and Trp^{190} in AnxA3. The tryptophan residues in AnxA4 and AnxA5 (Figure 8A) lie inside the protein core in a hydrophobic environment, as has been deduced from the crystal structures obtained in the absence of calcium bound in domain III [4,35]. The predicted model for AnxA13b also locates Trp^{227} in a hydrophobic buried environment.

Figure 8(B) shows the protein model predicted for the calcium-bound conformation of AnxA13b. The conformational change upon calcium binding can be observed through comparison of domain III in Figures 8(A) and 8(B). The main changes affect the regions involved in type II calcium-binding sites: the AB loop, with exposure of Trp^{227}, and helix D, which increases in length and positions Glu^{268} in the correct orientation to establish co-ordinations with calcium together with the carbonyl oxygens from Gly^{223}, Arg^{226} and Gly^{228} (located in the AB loop). Exposed tyrosine residues are shown in a 'ball-and-stick' style, and buried ones in a 'wire-frame' style.

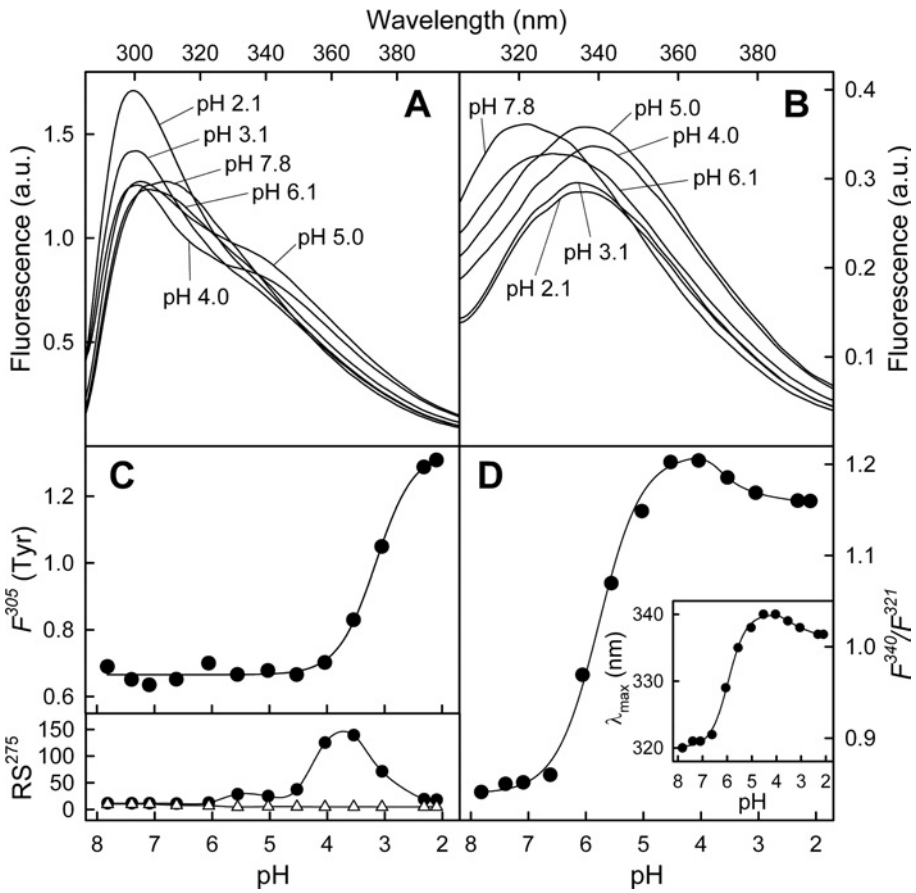

Figure 5 Fluorescence emission spectra of AnxA13b as a function of pH

Emission spectra at $\lambda_{ex} = 275$ nm (**A**) and $\lambda_{ex} = 295$ nm (**B**) at different pH values were registered at 20 °C; protein concentration was 0.05 mg/ml. Only representative spectra are shown. Fluorescence is expressed in arbitrary units (a.u.). Variations in the fluorescence intensity of tyrosine residues at 305 nm [F^{305} (Tyr); determined as described in the Experimental section] and in the F^{340}/F^{321} fluorescence intensity ratio of Trp^{227} ($\lambda_{ex} = 295$ nm) with pH are shown in (**C**) and (**D**) respectively. The lower panel in (**C**) represents Rayleigh scattering at 275 nm (RS^{275}) of AnxA13b (●) or buffer (△) at different pH values. The inset in (**D**) shows the variation in the tryptophan fluorescence maximum position with pH.

DISCUSSION

Analysis of the structure and function of AnxA13b is of great interest, as it is the founder member of the vertebrate family of annexins. It can be therefore considered as a prototype for conserved properties throughout the evolution of this superfamily of proteins [5,11]. Moreover, its specific pattern of expression and function in epithelial polarized cells presents some peculiarities in comparison with the rest of annexins, such as the binding to rafts [17–20]. In the present study, we wanted to gain insight into conformational changes induced by calcium binding, as well as by acidic pH, probably a shared characteristic among annexins. Additionally, we have studied the binding of AnxA13b, $AnxA13b^{myr}$ and $AnxA13^{core}$ to phospholipid vesicles, which could help us to understand its physiological functions and the essential role of the N-terminal region.

The overall secondary structure of AnxA13b is very similar to that reported for other annexins with a medium/short N-terminus, in which the mainly α-helical protein core has been described as a quite stable arrangement. However, the T_m of AnxA13b (44 °C) is the lowest reported to date among vertebrate annexins, only comparable with that of AnxA11 (45 °C) [28]. Interestingly, $AnxA13^{core}$ presents a T_m value approx. 6 °C higher than AnxA13b and is quite similar to that described for AnxA5 [31]. The great degree of structural similarity found in the protein core of the 'A' family, and the results of the present study for the $AnxA13^{core}$, indicate that differences in the N-terminus are probably the origin of the differences in thermal stability. In this case, the random-coil organization of this extension could induce a destabilization of the protein core, as we have previously reported for the long random coil N-terminus of AnxA11 [28]; AnxA1 and AnxA2, that possess N-termini similar in length to that of AnxA13b, but organized mainly in α-helical conformation, present a significantly higher T_m (approx. 60 °C in AnxA1) [36].

In contrast with the small effects that calcium binding seems to induce on the CD spectra, the T_m increases from 44 to approx. 55 °C when the calcium-binding sites in AnxA13b are saturated. This stabilization cannot be reproduced by the addition of magnesium. The T_m increase is similar to that observed for other annexins [31], and supports the notion that the interaction with calcium affects the whole protein core and is not limited to the binding sites, as suggested previously [32]. In any case, the calcium-bound conformation of AnxA13b shows a lower T_m than that of AnxA5 and AnxA11 (approx. 60 °C) [28,31].

AnxA13b presents only one tryptophan residue with a fluorescence emission maximum at 321 nm and barely accessible to acrylamide (K_{SV} of 2.99 M^{-1}). These data indicate that Trp^{227} is located in a hydrophobic cleft in the calcium-free conformation similar to Trp^{187} in AnxA5 [23,33,34] and in good accordance with the predicted three-dimensional model proposed for domain III of AnxA13b (Figure 8B). It has been reported that the hydrogen bond between Asp^{226} and Thr^{229} is essential for the stability of

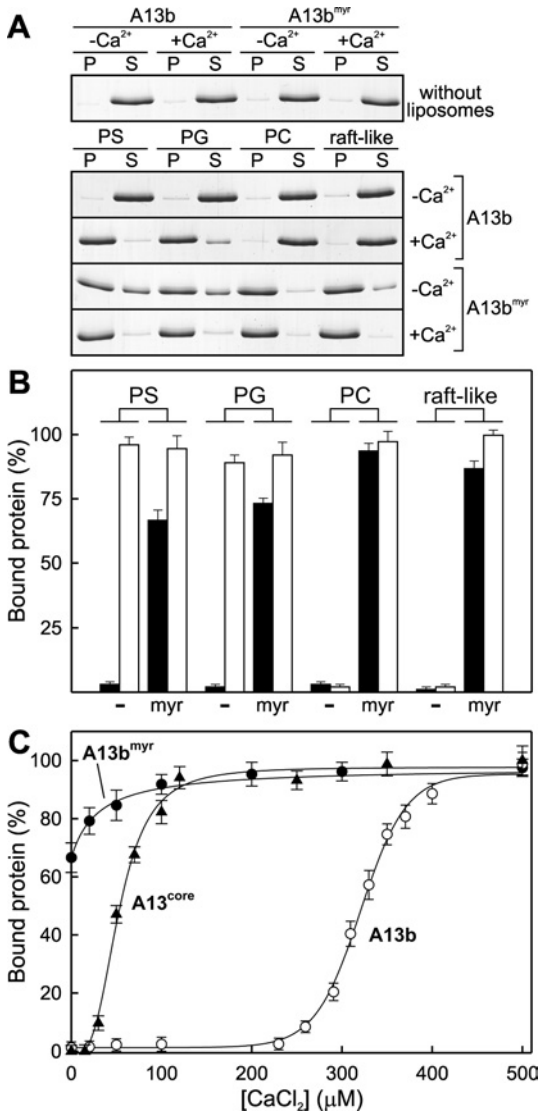

Figure 6 Binding of AnxA13b to liposomes with different lipid composition

The binding of AnxA13b to 400 nm unilamellar liposomes with different lipid composition [PS, PG, PC and PC/sphingomyelin/cholesterol, 1:1:1 (raft-like)] was performed by ultracentrifugation in the absence of calcium (1 mM EGTA; $-Ca^{2+}$ and closed bars) or in the presence of 500 μM $CaCl_2$ ($+Ca^{2+}$ and open bars) with a lipid/protein molar ratio of 800:1. (**A**) AnxA13b in the pellets (P) and in the supernatants (S) was analysed by SDS/PAGE followed by Coomassie Blue staining; representative gels are given. (**B**) Quantification of the binding of non-myristoylated (–) and myristoylated (myr) AnxA13b was carried out by densitometry of the gels or by radioactivity measurement of myristoylated AnxA13b. (**C**) Influence of calcium concentration on the binding of non-myristoylated (A13b; ○) and myristoylated ($A13b^{myr}$; ●) AnxA13b, and its protein core ($A13^{core}$; ▲) to 400 nm PS vesicles was analysed as in (**A**), but using $CaCl_2$ concentrations ranging from 0 (1 mM EGTA) to 500 μM. Data in (**B**) and (**C**) represent means ± S.D. for at least three independent experiments.

the closed conformation of domain III of AnxA5. This bond is broken after calcium binding or when pH is lowered with the consequent conformational rearrangement [33,34]. Interestingly, these residues have their equivalent in AnxA13b (Glu^{266} and Thr^{269}) and thus this interaction could take place in AnxA13b (Figure 8A). Taking into account that AnxA13b has been proposed as the founder member of vertebrate annexins [5,11], the closed conformation in domain III could be a conserved configuration inherited from ancient annexins and the constitutively open conformation in other annexins, such as AnxA3 and AnxA8, may reflect its adaptation to specific functions [37].

Whereas calcium binding does not modify the overall secondary structure of AnxA13b in the absence of phospholipids, the fluorescence emission spectrum of Trp^{227} is greatly altered as a result of a conformational change that affects the IIIA–IIIB loop. These changes in the tryptophan environment take place at lower calcium concentrations than those required for thermal stabilization, suggesting that calcium-binding sites different from the type II also contribute to the stabilization of the AnxA13b protein core. The emission maximum red-shift of 23 nm reflects the movement from a hydrophobic to a polar environment. Accordingly, the quenching constant increases to 14.58 M^{-1}, characteristic of an almost completely exposed tryptophan residue [38]. These observations can be explained by the rearrangement of the annexin fold, which only involves a minor modification in the overall secondary structure, but greatly alters the tryptophan environment, as described for AnxA5 [31,39]. However, the quantum yield of this residue is almost unaltered, even though the polar environment is a strong tryptophan quencher. Thus Trp^{187} is likely to be quenched already when it is buried in the hydrophobic cleft owing to the establishment of hydrogen bonds with Thr^{224} (Figure 8A) [34]. Even though AnxA13b does not present a threonine residue in this position (Ala^{246}), quenching of Trp^{227} could originate from a hydrogen bond with the carbonyl group of Ala^{246}, whose oxygen atom is close to the nitrogen in Trp^{227}.

As mentioned previously, the predicted three-dimensional model and the sequence alignment between AnxA13b and AnxA5 indicate that the former annexin presents only some of the stabilizing bonds that maintain the closed conformation. It can be therefore suggested that the AnxA13b calcium-free conformation is not as stable as that in AnxA5. In fact, we have observed that acidification induces a gradual shift in the Trp^{227} environment similar to that described upon calcium binding, with a midpoint effect at pH 5.8–5.9, whereas AnxA5 shows this effect at a more acidic pH value [27,33]. The alteration in Trp^{227} down to pH 4.1 is only accompanied by small secondary-structure changes that mainly affect the length of α-helices. If this structural change is similar to that reported for AnxA5 after calcium binding, an increase in the length of helices D could take place [34].

It has been suggested that the conformation acquired by AnxA5 and AnxB12 at mildly acidic pH may be an intermediate state for their calcium-independent binding to membranes under these conditions [40–43]. The N-terminal half of AnxA6 also presents a conformational change at acidic pH, but it involves a partial denaturation of the protein core with exposure of hydrophobic regions [44] that is not detected in annexins A5, A13b and B12. Moreover, site-directed spin labelling has revealed that AnxB12 inserts into the lipid bilayer after undergoing a profound structural reorganization in which the conformation described at mildly acidic pH may be an intermediate state [41,43,45]. This conserved characteristic between *Hydra* and vertebrate annexins could be a consequence of convergent evolution or could well be a common ancestral property of all annexins. AnxA13b (more related to non-vertebrate and ancient annexins) shows this acidic pH-triggered rearrangement in solution, which strongly argues for the latter assumption. As a whole, these observations suggest the presence of a proton-dependent switch in annexins which harbours the information to induce membrane insertion. This insertion could explain some of the physiological properties of these proteins, such as calcium channel activity, and could also underlie its pathway of secretion.

We have found that AnxA13b maintains the phospholipid specificity, but requires much higher calcium concentrations than those described for the rest of the annexins [1–3,9]. This finding is quite surprising considering that the more calcium accessible open conformation should be favoured in the proximity of anionic

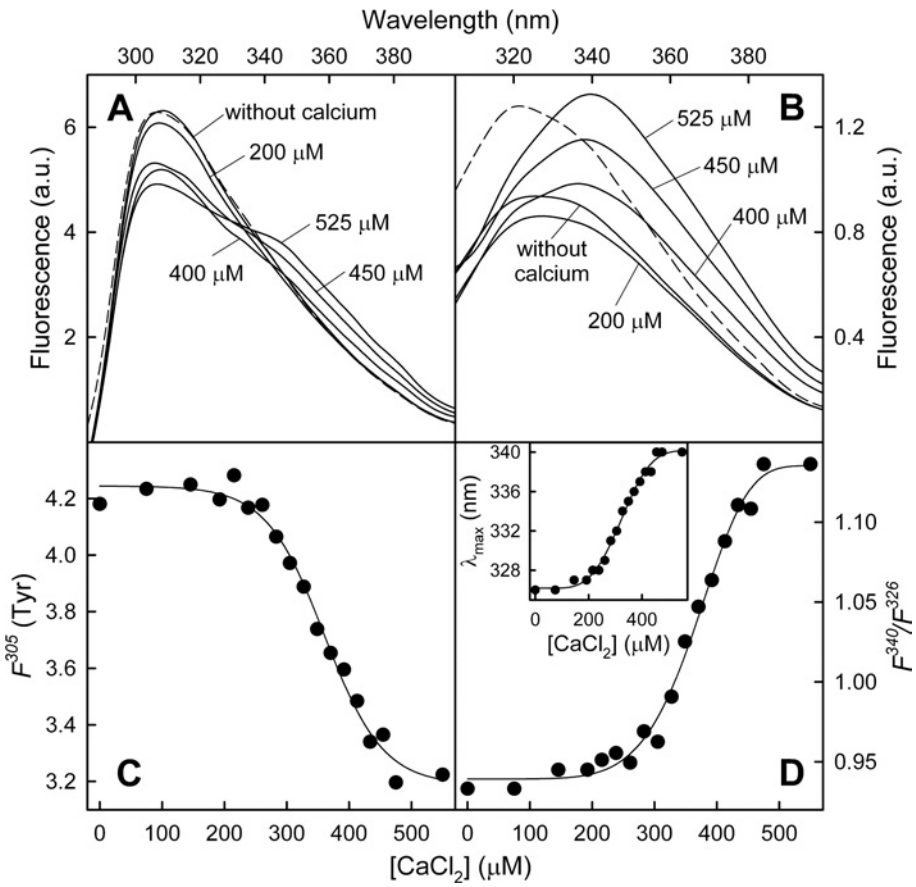

Figure 7 Calcium-dependent changes in the fluorescence emission spectra of AnxA13b in the presence of PS liposomes

Emission spectra at $\lambda_{ex} = 275$ nm (**A**) and $\lambda_{ex} = 295$ nm (**B**) in the absence of calcium or at increasing $CaCl_2$ concentration were registered at 20 °C in the presence of 50 nm unilamellar PS vesicles using a lipid/protein molar ratio of 800:1 (protein concentration: 0.2 mg/ml or 5 μM). The broken line represents the spectra in the absence of calcium and PS. Only representative calcium concentrations and spectra are shown. Fluorescence is expressed in arbitrary units (a.u.). Variations in the fluorescence intensity of tyrosine residues at 305 nm [F^{305} (Tyr); determined as described in the Experimental section] and in the F^{340}/F^{326} fluorescence intensity ratio of Trp^{227} ($\lambda_{ex} = 295$ nm) with calcium concentration are shown in (**C**) and (**D**) respectively. The inset in (**D**) shows the variation in the tryptophan fluorescence maximum position with calcium concentration.

phospholipids (local pH decrease of approx. 1.6 units [46]) and that the annexin core is highly homologous. Thus changes in the protein sequence are not likely to be responsible for this low affinity. In consequence, the relatively long AnxA13b N-terminus could interact with the protein core, inducing both the loss in stability (low T_m) and the high calcium requirement for binding to liposomes. This hypothesis is strongly supported by the fact that truncated $AnxA13^{core}$ not only presents significantly higher thermal stability than the intact molecule, but also has much lower calcium requirements for binding to PS vesicles.

Addition of PS vesicles to AnxA13b in the absence of calcium induces an alteration in the fluorescence emission spectrum of Trp^{227} and in the CD spectrum similar to those observed when the pH is lowered. This change could be explained by the already mentioned effect of anionic phospholipids in the pH near the surface of the membrane [46]. Subsequent addition of calcium initially induces a red-shift in the fluorescence maximum, with a midpoint effect at the same calcium concentration required for 50 % binding, followed by an increase in the Trp^{227} quantum yield. The requirement for an initial nucleation step could be responsible for this sequential modification of the spectrum. Additionally, we have observed by CD spectroscopy that binding of AnxA13b to PS liposomes induces a structural rearrangement, which mainly affects the length of α-helices, that is accompanied by a large increase (approx. 25 °C) in the T_m, in a similar pattern to what we have reported previously for AnxA11 [28].

Regarding the variation in tyrosine emission spectra with calcium concentration in the presence of PS, a decrease in the quantum yield of these residues is observed almost in parallel with the alteration in the tryptophan residue. This sigmoid decrease is not observed in the absence of PS or when the pH is decreased. Thus it is highly probable that this alteration in tyrosine fluorescence is not directly due to the conformational change that takes place upon calcium binding (open conformation), but is more probably due to the establishment of interactions between annexin molecules on the surface of the liposomes. In fact, according to the model proposed in Figure 8(B), Tyr^{101} and Tyr^{220} are highly exposed residues located in regions equivalent to those described in AnxA5 to play a key role in its self-assembly on the surface of the membranes [47]. Taking into account the similarities between these two annexins, the mentioned tyrosine residues would change to a less hydrophilic environment, probably forming hydrogen bonds that are responsible for the static quenching of the fluorescence emission.

The high calcium concentrations required for the binding of recombinant AnxA13b to membranes are never achieved under physiological conditions inside the cell. In addition, we have only detected calcium-dependent binding of AnxA13b to acidic

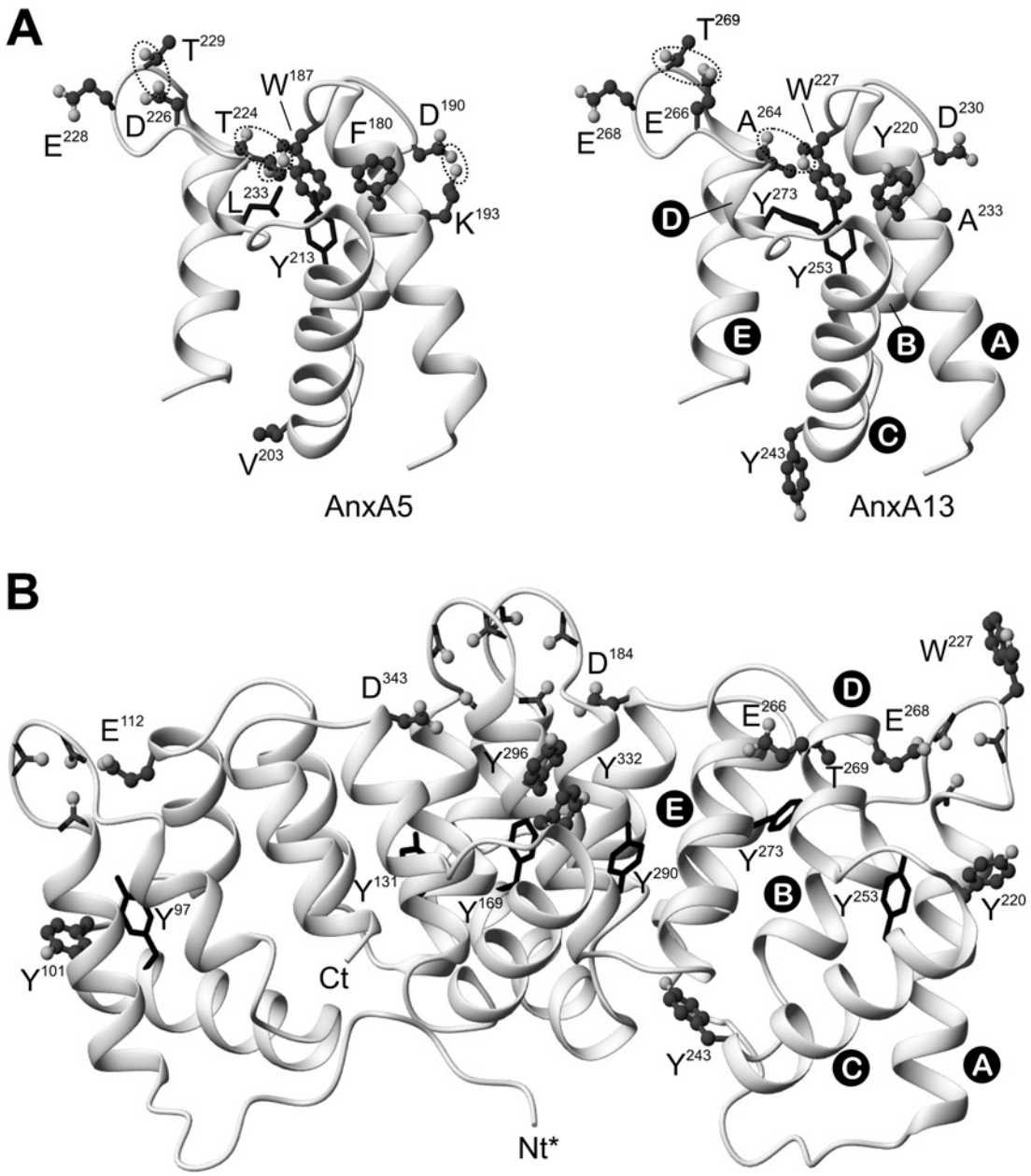

Figure 8 AnxA13b three-dimensional model

Three-dimensional protein models of human AnxA13b were derived by sequence threading through X-ray crystallography co-ordinates of different annexins using the Swiss-Model Server version 3.5. (**A**) Comparison of the three-dimensional structure of domain III of human AnxA5 with that predicted for AnxA13 in the absence of calcium bound to this domain (closed conformation). Dotted lines mark hydrogen bonds or salt bridges essential for the maintenance of the closed calcium-free conformation. (**B**) Three-dimensional protein model of AnxA13b (residues 44–357) in the 'high-calcium' form. Nt*, residues 1–43 from the non-homologous N-terminal domain of AnxA13b are not shown. Ct, C-terminus. Tyrosine residues are represented in a wire-frame style if they are predicted as buried or in a ball-and-stick style if they are exposed to the solvent. The four major calcium co-ordination sites are located on the upper convex surface; the carbonyl groups and acid residues proposed to be involved in calcium co-ordination are shown together with some additional residues commented on in the text. Helix nomenclature in domain III is shown. Note that the orientation of domain III is not the same in (**A**) and (**B**) to facilitate the view of the stabilizing bonds in the closed conformation. The Figure was prepared using the MOLMOL program [48].

phospholipids (PS and PG), but not to neutral ones (PC) or to raft-like liposomes. On the other hand, it has been described that this protein binds to rafts *in vivo*, and that this interaction is essential for its functionality [19,20]. The only difference between recombinant and wild-type AnxA13b is N-myristoylation; therefore this post-translational modification must be responsible for binding to lipid rafts. AnxA13b^{myr} binds in a calcium-independent manner to acidic phospholipids (more than 70 %) and to PC and raft-like liposomes, confirming the essential role of N-terminal myristoylation of this annexin for its *in vivo* function. Even though it has been reported that AnxA13a and AnxA13b bind in a calcium-independent manner to membranes, and that myristoylation is required for this binding [20], these studies were performed using membrane extracts from cells transfected with wild-type and non-myristoylated mutants of these proteins. Thus this is the first time that a direct interaction between myristoylated

AnxA13b and neutral and raft-like structures has been shown, without disregarding that other proteins may modulate this interaction.

We have performed for the first time an exhaustive spectroscopical/structural characterization of AnxA13b, the oldest vertebrate annexin with the most tissue-specific expression. This ancient annexin, more related to invertebrate or even protist and plant annexins, presents some structural features that have been conserved during the evolution of vertebrate annexins. Thus forces stabilizing the closed calcium-free conformation, the structural changes upon calcium binding and the acidic pH conformational switch detected in quite modern annexins (such as AnxA5) are likely to be conserved properties that are inherited from ancestral annexins and are not the result of a convergent evolution. On the other hand, it is noteworthy that the N-terminus of this annexin presents unique properties, not only because of alternative splicing that yields two isoforms with different functionality regarding membrane trafficking, but also because it is N-myristoylated. This post-translational modification probably alters the structure and stability of the highly conserved protein core, as we have observed that the non-myristoylated protein is relatively unstable compared with its protein core and with other vertebrate annexins. However, the most surprising finding has been the high calcium requirements that the non-myristoylated protein presents; this impairment disappears upon N-myristoylation. This unique structural feature enables AnxA13b to interact directly, in a calcium-independent manner, with raft-like domains, an interaction that is essential for its *in vivo* functionality.

This work was supported by the Spanish grant BMC2002-01407 and BMC2002-00827 from Dirección General de Investigación. A.G.-A. has been recipient of the Spanish fellowship Severo Ochoa from the Ferrer Research Group.

REFERENCES

1 Raynal, P. and Pollard, H. B. (1994) Annexins: the problem of assessing the biological role for a gene family of multifunctional calcium- and phospholipid-binding proteins. Biochim. Biophys. Acta **1197**, 63–93

2 Swairjo, M. A. and Seaton, B. A. (1994) Annexin structure and membrane interactions: a molecular perspective. Annu. Rev. Biophys. Struct. **23**, 193–213

3 Gerke, V. and Moss, S. E. (2002) Annexins: from structure to function. Physiol. Rev. **82**, 331–371

4 Liemann, S. and Huber, R. (1997) Three-dimensional structure of annexins. Cell. Mol. Life Sci. **53**, 516–521

5 Fernandez, M. P. and Morgan, R. O. (2003) Structure, function and evolution of the annexin supergene family. In Annexins: Biological Importance and Annexin-Related Pathologies (Bandorowicz-Pikula, J., ed.), pp. 21–37, Landes Bioscience, Georgetown

6 Huber, R., Römisch, J. and Pâques, E. P. (1990) The crystal and molecular structure of human annexin V, an anticoagulant protein that binds to calcium and membranes. EMBO J. **9**, 3867–3873

7 Patel, D. R., Jao, C. C., Mailliard, W. S., Isas, J. M., Langen, R. and Haigler, H. T. (2001) Calcium-dependent binding of annexin 12 to phospholipid bilayers: stoichiometry and implications. Biochemistry **40**, 7054–7060

8 Montaville, P., Neumann, J., Russo-Marie, F., Oschenbein, F. and Saison, A. (2002) A new consensus sequence for phosphatidylserine recognition by annexins. J. Biol. Chem. **277**, 24684–24693

9 Turnay, J., Guzmán-Aránguez, A., Lecona, E., Pérez-Ramos, P., Fernández-Lizarbe, S., Olmo, N. and Lizarbe, M. A. (2003) Influence of the N-terminal domain of annexins in their functional properties. Recent Res. Dev. Biochem. **4**, 53–78

10 Turnay, J., Lecona, E., Guzmán-Aránguez, A., Pérez-Ramos, P., Fernández-Lizarbe, S., Olmo, N. and Lizarbe, M. A. (2003) Annexins: structural characteristics of the N-terminus and influence on the overall structure of the protein. Recent Res. Dev. Biochem. **4**, 79–95

11 Morgan, R. O. and Fernandez, M. P. (1997) Distinct annexin subfamilies in plants and protists diverged prior to animal annexins and from a common ancestor. J. Mol. Evol. **44**, 178–188

12 Morgan, R. O., Bell, D. W., Testa, J. R. and Fernandez, M. P. (1998) Genomic locations of ANX11 and ANX13 and the evolutionary genetics of human annexins. Genomics **48**, 100–110

13 Bances, P., Fernández, M. R., Rodríguez-García, M. I., Morgan, R. O. and Fernandez, M. P. (2000) Annexin A11 (ANXA11) gene structure as the progenitor of paralogous annexins and source of orthologous cDNA isoforms. Genomics **69**, 95–103

14 Iglesias, J. M., Morgan, R. O., Jenkins, N. A., Copeland, N. G., Gilbert, D. J. and Fernandez, M. P. (2002) Comparative genetics and evolution of annexin A13 as the founder gene of vertebrate annexins. Mol. Biol. Evol. **19**, 608–618

15 Wice, B. M. and Gordon, J. I. (1992) A strategy for isolation of cDNAs encoding proteins affecting human intestinal epithelial cell growth and differentiation: characterization of a novel gut-specific N-myristoylated annexin. J. Cell Biol. **116**, 405–422

16 Fiedler, K., Lafont, F., Parton, R. G. and Simons, K. (1995) Annexin XIIIb: a novel epithelial specific annexin is implicated in vesicular traffic to the apical plasma membrane. J. Cell Biol. **128**, 1043–1053

17 Massey-Harroche, D., Mayran, N. and Maroux, S. (1998) Polarized localizations of annexins I, II, VI and XIII in epithelial cells of intestinal, hepatic and pancreatic tissues. J. Cell Sci. **111**, 3007–3015

18 Massey-Harroche, D. (2000) Epithelial cell polarity as reflected in enterocytes. Microsc. Res. Tech. **49**, 353–362

19 Lafont, F., Lecat, S., Verkade, P. and Simons, K. (1998) Annexin XIIIb associates with lipid microdomains to function in apical delivery. J. Cell Biol. **142**, 1413–1427

20 Lecat, S., Verkade, P., Thiele, C., Fiedler, K., Simons, K. and Lafont, F. (2000) Different properties of two isoforms of annexin XIII in MDCK cells. J. Cell Sci. **113**, 2607–2618

21 Noda, Y., Okada, Y., Saito, N., Setou, M., Xu, Y., Zheizeng, Z. and Hirokawa, N. (2001) KIFC3, a microtubule minus end-directed motor for the apical transport of annexin XIIIb-associated Triton-insoluble membranes. J. Cell Biol. **155**, 77–88

22 Plant, P. J., Lafont, F., Lecat, S., Verkade, P., Simons, K. and Rotin, D. (2000) Apical membrane targeting of Nedd4 is mediated by an association of its C2 domain with annexin XIIIb. J. Cell Biol. **149**, 1473–1483

23 Arboledas, D., Olmo, N., Lizarbe, M. A. and Turnay, J. (1997) Role of the N-terminus in the structure and stability of chicken annexin V. FEBS Lett. **416**, 217–220

24 Duronio, R. J., Jackson-Machelski, E., Heuckeroth, R. O., Olins, P. O., Devine, C. S., Yonemoto, W., Slice, L. W., Taylor, S. S. and Gordon, J. I. (1990) Protein N-myristoylation in *Escherichia coli*: reconstitution of a eukaryotic protein modification in bacteria. Proc. Natl. Acad. Sci. U.S.A. **87**, 1506–1510

25 Gómez-Gutiérrez, J., Rodríguez-Crespo, I., Peterson, D. L. and Gavilanes, F. (1994) Reconstitution of hepatitis B surface antigen proteins into phospholipid vesicles. Biochim. Biophys. Acta **1192**, 45–52

26 Perczel, A., Park, K. and Fasman, G. D. (1992) Analysis of the circular dichroism spectrum of proteins using the convex constraint algorithm: a practical guide. Anal. Biochem. **203**, 83–93

27 Beermann ofm cap, B. B., Hinz, H.-J., Hofmann, A. and Huber, R. (1998) Acid induced equilibrium unfolding of annexin V wild type shows two intermediate states. FEBS Lett. **423**, 265–269

28 Lecona, E., Turnay, J., Olmo, N., Guzmán-Aránguez, A., Morgan, R. O., Fernandez, M. P. and Lizarbe, M. A. (2003) Structural and functional characterization of recombinant mouse annexin A11: influence of calcium binding. Biochem. J. **373**, 437–449

29 Laemmli, U. K. (1970) Cleavage of structural proteins during the assembly of the head of bacteriophage T4. Nature (London) **227**, 680–685

30 Campos, B., Mo, Y. D., Mealy, T. R., Li, C. W., Swairjo, M. A., Balch, C., Head, J. F., Retzinger, G., Dedman, J. R. and Seaton, B. A. (1998) Mutational and crystallographic analyses of interfacial residues in annexin V suggest direct interactions with phospholipid membrane components. Biochemistry **37**, 8004–8010

31 Turnay, J., Olmo, N., Gasset, M., Iloro, I., Arrondo, J. L. R. and Lizarbe, M. A. (2002) Calcium-dependent conformational rearrangements and protein stability in chicken annexin A5. Biophys. J. **83**, 2280–2291

32 Ayala-Sanmartin, J., Vincent, M., Sopkova, J. and Gallay, J. (2000) Modulation by Ca^{2+} and by membrane binding of the dynamics of domain III of annexin 2 (p36) and the annexin 2–p11 complex (p90): implications for their biochemical properties. Biochemistry **39**, 15179–15189

33 Sopkova, J., Vincent, M., Takahashi, M., Lewit-Bentley, A. and Gallay, J. (1998) Conformational flexibility of domain III of annexin V studied by fluorescence of tryptophan 187 and circular dichroism: the effect of pH. Biochemistry **37**, 11962–11970

34 Sopková-De Oliveira Santos, J., Vincent, M., Tabaries, S., Chevalier, A., Kerboeuf, D., Russo-Marie, F., Lewit-Bentley, A. and Gallay, J. (2001) Annexin A5 D226K structure and dynamics: identification of a molecular switch for the large-scale conformational change of domain III. FEBS Lett. **493**, 122–128

35 Zanotti, G., Malpeli, G., Gliubich, F., Folli, C., Stoppini, M., Olivi, L., Savoia, A. and Berni, R. (1998) Structure of the trigonal crystal form of bovine annexin IV. Biochem. J. **329**, 101–106

36 Rosengarth, A., Rösgen, J., Hinz, H.-J. and Gerke, V. (1999) A comparison of the energetics of annexin I and annexin V.J. Mol. Biol. **288**, 1013–1025

37 Réty, S., Sopková-de Oliveira Santos, J., Dreyfuss, L., Blondeau, K., Hofbaurová, K., Raguénès-Nicol, C., Kerbouef, D., Renouard, M., Russo-Marie, F. and Lewitt-Bentley, A. (2005) The crystal structure of annexin A8 is similar to that of annexin A3. J. Mol. Biol. **345**, 1131–1139.

38 Lakowicz, J. R. (1999) Quenching of fluorescence. In Principles of Fluorescence Spectroscopy, 2nd edn. (Lakowicz, J. R., ed.), pp. 237–265, Kluwer Academic/Plenum Publishers, New York
39 Sopkova, J., Gallay, J., Vincent, M., Pancoska, P. and Lewit-Bentley, A. (1994) The dynamic behavior of annexin V as a function of calcium ion binding: a circular dichroism, UV absorption, and steady-state and time-resolved fluorescence study. Biochemistry **33**, 4490–4499
40 Kohler, G., Hering, U., Zschoring, O. and Arnold, K. (1997) Annexin V interaction with phosphatidylserine-containing vesicles at low and neutral pH. Biochemistry **36**, 8189–8194
41 Langen, R., Isas, J. M., Hubbell, W. L. and Haigler, H. T. (1998) A transmembrane form of annexin XII detected by site-directed spin labeling. Proc. Natl. Acad. Sci. U.S.A. **95**, 14060–14065
42 Isas, J. M., Cartailler, J. P., Sokolov, Y., Patel, D. R., Langen, R., Luecke, H., Hall, J. E. and Haigler, H. T. (2000) Annexins V and XII insert into bilayers at mildly acidic pH and form ion channels. Biochemistry **39**, 3015–3022

Received 18 November 2004/6 April 2005; accepted 7 April 2005
Published as BJ Immediate Publication 7 April 2005, DOI 10.1042/BJ20041918

43 Ladokhin, A. S. and Haigler, H. T. (2005) Reversible transition between the surface trimer and membrane-inserted monomer of annexin 12. Biochemistry **44**, 3402–3409
44 Golczak, M., Kirilenko, A., Bandorowicz-Pikula, J., Desbat, B. and Pikula, S. (2004) Structure of human annexin A6 at the air–water interface and in a membrane-bound state. Biophys. J. **87**, 1215–1226
45 Isas, J. M., Patel, D. R., Jao, C., Jayasinghe, S., Cartailler, J., Haigler, H. T. and Langen, R. (2003) Global structural changes in annexin 12: the roles of phospholipid, Ca^{2+}, and pH. J. Biol. Chem. **278**, 30227–30234
46 Van der Goot, F. G., González-Mañas, J. M., Lakey, J. H. and Pattus, F. (1991) A 'molten-globule' membrane-insertion intermediate of the pore-forming domain of colicin A. Nature (London) **354**, 408–410
47 Oling, F., Bergsma-Schutter, W. and Brisson, A. (2001) Trimers, dimers of trimers, and trimers of trimers are common building blocks of annexin A5 two-dimensional crystals. J. Struct. Biol. **133**, 55–63
48 Koradi, R., Billeter, M. and Wüthrich, K. (1996) MOLMOL: a program for display and analysis of macromolecular structures. J. Mol. Graphics **14**, 51–55